Available at
http://pvamu.edu/aam
Appl. Appl. Math.
ISSN: 1932-9466

Applications and Applied Mathematics:
An International Journal
(AAM)

Special Issue No. 4 (March 2019), pp. 54 – 68

MHD Flow of Tangent Hyperbolic Nanofluid over an Inclined Sheet with Effects of Thermal Radiation and Heat Source/Sink

[1]N. Saidulu, [2]T. Gangaiah, and [3]A. Venkata Lakshmi

Department of Mathematics
Osmania University
Hyderabad-500 007
Telangana, India
[1]nampellysaidulu28@gmail.com, [2]tgangaiah79@gmail.com, [3]akavaramvlr@gmail.com

Received: August 8, 2018; Accepted: October 28, 2018

Abstract

This article presents the effect of thermal radiation on MHD boundary layer flow of tangent hyperbolic fluid with nanoparticles past an inclined stretching sheet with heat source/sink and convective boundary condition. Condition of zero normal flux of nanoparticles at the wall is used for the concentration boundary condition, which is the current topic that have yet to be studied extensively. The partial differential systems are reduced to ordinary differential systems by using appropriate similarity transformations. The reduced systems are solved numerically by Runge-Kutta fourth order method with shooting technique. The velocity, temperature and nanoparticle volume fraction profiles are discussed for different physical parameters. As well as the Skin friction coefficient, Nusselt number and Sherwood numbers have discussed in detail and presented through graphically. It is found that the thermal radiation enhances the effective thermal diffusivity and the temperature rises. It is also observed that the buoyancy parameter strengthens the velocity field, showing a decreasing behavior of temperature and nanoparticle volume fraction profiles.

Keywords: MHD; tangent hyperbolic; thermal radiation; mixed convection; inclined sheet

MSC 2010 No.: 76A10, 76D99, 76W05, 80A20

1. Introduction

The momentum and heat transfer of the boundary layer flow over a stretching surface have been applied in numerous chemical engineering processes, such as polymer extrusion processes and met-

allurgical processes, which involve cooling of a molten liquid. Sakiadis (1961) initiated studying the boundary layer flow over a stretched surface moving with a constant velocity and formulated boundary layer equations for two dimensional and axisymmetric flows. Crane (1970) investigated the flow caused by a stretching sheet. On the other hand, Gupta and Gupta (1977) stressed that realistically, stretching surface is not necessarily continuous. Magyari and Keller (1999) analyzed the steady boundary layers on an exponentially stretching continuous surface with an exponential temperature distribution. Elbashbeshy (2001) investigated the heat transfer over an exponentially stretching continuous surface with suction. Fathizadeh et al. (2011) proposed a powerful modification of the homotopy perturbation method for MHD flow over a stretching sheet. Bhattacharyya et al. (2013) analyzed the similarity solution of mixed convective boundary layer flow towards a vertical surface with slip conditions. The analytical solution of mixed convection boundary layer flow of micropolar fluid over a heated shrinking surface was investigated by Rashidi et al. (2013). Hayat et al. (2014) studied the mixed convective two-dimensional flow due to a vertical porous plate. The flow analysis was carried out in the presence of variable thermal conductivity and convective boundary condition.

The most important non-Newtonian fluid model is a tangent hyperbolic fluid model and which has certain advantages over other non-Newtonian formulations. Pop and Ingham (2001) presented the tangent hyperbolic fluid model and it is extensively used in different laboratory experiments. After that, Nadeem and Akram (2009) studied the peristaltic transport of a hyperbolic tangent fluid within an asymmetric channel. The tangent hyperbolic fluid model is used by Friedman et al. (2013) for large-scale magneto-rheological fluid damper coils. In another study, peristaltic flow of tangent hyperbolic fluid in a curved channel is studied by Nadeem and Maraj (2013) and they explored the behavior of various parameters on pressure rise against flow rate and plotted stream lines to understand the pattern of the flow. Akbar et al. (2013) investigated the steady MHD flow of tangent hyperbolic fluid over a stretching sheet. They found that velocity profile decreases by increasing power law index and Weissenberg number but demonstrates opposite results for skin friction.

A nanofluid is a liquid containing nanometer-sized solid particles, called nanoparticles, which basically enhancing thermal conductivity of the base fluids according to an investigation of Choi (1995). Pak and Cho (1998) ascribed the increased heat transfer coefficients noticed in nanofluids to the dispersion of suspended particles. Xuan and Li (2003) proposed that the heat transfer enhancement was the result of the increase in turbulence induced by nanoparticle motion. Wang and Wei (2009) show that macroscale heat conduction in nanofluids is of a dual-phase-lagging type rather than the Fourier type. This leads to models for effective thermal capacity, conductivity and diffusivity of nanofluids and reveals even more anomalous thermal behavior of nanofluids. Due to the significant enhancing thermal conductivity property, nanofluids have huge advantages over ordinary fluids. In packaging and plastic industry, incorporation of nanoparticles can play a vital role on the quality and strength of final product. Following this pioneering work, Buongiorno (2010) proposed a model in which seven slip mechanism is considered namely, inertia, Brownian diffusion, thermophoresis, diffusionphoresis, Magnus effect, fluid drainage and gravity settling and according to him absolute velocity can be viewed as the sum of the base fluids velocity and a relative velocity. In this model he has not considered the effects of shape of nanoparticles.

Kuznetsov and Nield (2010) have investigated the natural convective boundary layer flow of a nanofluid past a vertical plate analytically. In this study they used a model for nanofluid that incorporates the Brownian motion and thermophoresis effects. Using the same model Khan and Pop (2010) studied the boundary layer flow of a nanofluid over a stretching sheet with a constant surface temperature. Kuznetsov and Nield (2014) reinvestigated their existing model and revised a model for both active and zero flux of nanoparticle at the surface. In such conditions, they argued this model is more physically realistic as compared to the earlier model. Akram and Nadeem (2014) investigated the impact of peristaltic transport of a tangent hyperbolic fluid in the presence of nanoparticles under the influence of inclined magnetic field. They have found that increase in the Brownian motion and thermophoresis leads to enhance temperature profile. Sajjad et al. (2016) investigated the entropy generation via two important slip mechanism Brownian motion and thermophoresis diffusion in non-Newtonian nanofluid flow with zero normal flux of nanoparticles at the stretching surface. Bala (2016) investigated the theoretical study of the steady two-dimensional MHD convective boundary layer flow of a Casson fluid over an exponentially inclined permeable stretching surface in the presence of thermal radiation and chemical reaction. Prabhakar et al. (2016) analyzed the effect of inclined Lorentz forces on hyperbolic tangent nanofluid flow with zero normal flux of nanoparticles at the stretching sheet. Recently, many researchers discussed the tangent hyperbolic fluid flows over stretching surfaces (Hayat et al. (2016); Hayat et al. (2017); Salahuddin et al. (2017); Waqas et al. (2017); Mair et al. (2017); Kumar et al. (2017); Wubshet (2017)).

The aim of this present study is to investigate the condition of zero normal flux for tangent hyperbolic fluid over an inclined stretching sheet with the effects of radiation, heat source/sink and convective boundary condition. In the view of inclined stretching sheet, mathematical model is constructed by incorporating the Brownian motion and thermophoresis effects. This article is categorized in the following manner. In Section 2, tensor generation of tangent hyperbolic is performed and a complete mathematical model is structured for non-Newtonian fluid in the presence of slip mechanism of nanofluid. To discard the gravitational settling at the surface of the sheet, we have considered the passive control of nanoparticles at the surface which are defined in the boundary condition. In Section 4, results are determined for each velocity, temperature and nanoparticle volume fraction profiles with the help of numerical technique and these results are further described physically against each emerging parameter. In Section 5, a conclusion is drawn under the whole analysis.

2. Mathematical formulation

Consider the boundary layer flow of an incompressible viscous and electrically conducting tangent hyperbolic nanofluid flow over an inclined stretching surface which coincides with the plane $y = 0$. The fluid flow is confined to $y > 0$. The x-axis is taken along the continuous stretching sheet in the direction of motion while the y-axis is perpendicular to the sheet. Two equal and opposite forces are applied along the x-axis so that the wall is stretched keeping the origin fixed. The flow is assumed to be generated by stretching of the elastic boundary sheet from a slit with a large force such that the velocity of the boundary sheet is an exponential order of the flow directional coordinate x. Along with this we considered thermal radiation and heat source/sink to the flow. The flow takes

place in the upper half plane $y > 0$. A variable magnetic field $B(x)$ is applied normal to the sheet.

The constitutive equation of tangent hyperbolic fluid is (Nadeem and Akram (2009)):

$$\bar{\tau} = \left[\mu_\infty + (\mu_0 + \mu_\infty) \tanh\left(\Gamma\bar{\dot{\gamma}}\right)^n\right] \bar{\dot{\gamma}}. \tag{1}$$

In the above expression $\bar{\tau}$ is an extra stress tensor, μ_∞ is an infinite shear rate viscosity, μ_0 is the zero shear rate viscosity, Γ is the time-dependent material constant, n is the power law index, i.e. flow-behavior index, and $\bar{\dot{\gamma}}$ defined as:

$$\bar{\dot{\gamma}} = \sqrt{\frac{1}{2}\sum_i \sum_j \bar{\dot{\gamma}}_{ij}\bar{\dot{\gamma}}_{ji}} = \sqrt{\frac{1}{2}\Pi}, \tag{2}$$

where $\Pi = \frac{1}{2}tr\Big(\text{grad}V + (\text{grad}V)^T\Big)^2$. We consider Equation 1 for the case when $\mu_\infty = 0$ because it is not possible to discuss the problem for the infinite shear rate viscosity and since we are considering tangent hyperbolic fluid that describing shear thinning effects so $\Gamma\bar{\dot{\gamma}} < 1$. Then Equation 1 takes the following form:

$$\begin{aligned} \bar{\tau} &= \mu_0 \left[\left(\Gamma\bar{\dot{\gamma}}\right)^n\right] \bar{\dot{\gamma}} \\ &= \mu_0 \left[\left(1 + \Gamma\bar{\dot{\gamma}} - 1\right)^n\right] \bar{\dot{\gamma}} \\ &= \mu_0 \left[1 + n\left(\Gamma\bar{\dot{\gamma}} - 1\right)\right] \bar{\dot{\gamma}}. \end{aligned} \tag{3}$$

The governing equations for the tangent hyperbolic nanofluid model after applying the boundary layer approximations can be defined as follows:

$$\frac{\partial u}{\partial x} + \frac{\partial v}{\partial y} = 0, \tag{4}$$

$$\begin{aligned} u\frac{\partial u}{\partial x} + v\frac{\partial u}{\partial y} =& \nu\left(1 - n\right)\frac{\partial^2 u}{\partial y^2} + \sqrt{2}\nu n\Gamma\left(\frac{\partial u}{\partial y}\right)\frac{\partial^2 u}{\partial y^2} \\ &+ \left[g\beta_T\left(T - T_\infty\right) + g\beta_C\left(C - C_\infty\right)\right]\sin\gamma - \frac{\sigma B^2}{\rho}u, \end{aligned} \tag{5}$$

$$u\frac{\partial T}{\partial x} + v\frac{\partial T}{\partial y} = \frac{k}{\rho c_p}\frac{\partial^2 T}{\partial y^2} - \frac{1}{\rho c_p}\frac{\partial q_r}{\partial y} + \tau\left\{D_B\frac{\partial C}{\partial y}\frac{\partial T}{\partial y} + \frac{D_T}{T_\infty}\left(\frac{\partial T}{\partial y}\right)^2\right\} + \frac{Q}{\rho c_p}\left(T - T_\infty\right), \tag{6}$$

$$u\frac{\partial C}{\partial x} + v\frac{\partial C}{\partial y} = D_B\frac{\partial^2 C}{\partial y^2} + \left(\frac{D_T}{T_\infty}\right)\frac{\partial^2 T}{\partial y^2}, \tag{7}$$

where u and v are the velocities in the x- and y-directions, respectively, $\nu = \frac{\mu}{\rho}$ is the kinematic viscosity, ρ is the fluid density (assumed constant), μ is the coefficient of fluid viscosity, σ is the electrical conductivity, g is an acceleration due to gravity, β_T is the coefficient of thermal expansion, β_C is the coefficient of solutal expansion, γ is an inclination angle, k is the thermal conductivity, T is the fluid temperature, T_∞ is constant temperature of the fluid in the viscid free stream, q_r is the radiative heat flux, c_p is the specific heat at constant pressure, $\tau = \frac{(\rho c)_p}{(\rho c)_f}$ is the ratio between the effective heat capacity of the nanoparticle material to the heat capacity of the base fluid, ρ_p is the density of the particles, c_f is the volumetric expansion coefficient, C is the nanoparticle volume fraction, D_B is the Brownian diffusion coefficient, and D_T is the thermophoretic diffusion coefficient. Q is the dimensional heat generation ($Q > 0$) or absorption ($Q < 0$) coefficient.

In writing Equation (5), we have neglected the induced magnetic field since the magnetic Reynolds number for the flow is assumed to be very small.

Using Rosseland approximation for radiation we can write

$$q_r = -\frac{4\delta^*}{3k^*}\frac{\partial T^4}{\partial y}, \tag{8}$$

where δ^* is the Stefan-Boltzman constant, k^* is the absorption coefficient. Assuming that T^4 is a linear function of temperature, then

$$T^4 = 4T_\infty^3 T - 3T_\infty^4. \tag{9}$$

Using Equation (8) and (9), Equation (6) reduces to:

$$u\frac{\partial T}{\partial x} + v\frac{\partial T}{\partial y} = \frac{k}{\rho c_p}\frac{\partial^2 T}{\partial y^2} + \frac{16\delta^* T_\infty^3}{3\rho c_p k^*}\frac{\partial^2 T}{\partial y^2} + \tau\left\{D_B\frac{\partial C}{\partial y}\frac{\partial T}{\partial y} + \frac{D_T}{T_\infty}\left(\frac{\partial T}{\partial y}\right)^2\right\} + \frac{Q}{\rho c_p}\left(T - T_\infty\right). \tag{10}$$

2.1. Boundary conditions

The appropriate boundary conditions for the problem are given by

$$u = U, \quad v = -V, \quad -k\frac{\partial T}{\partial y} = h_f\left(T_f - T\right), \quad D_B\frac{\partial C}{\partial y} + \frac{D_T}{T_\infty}\frac{\partial T}{\partial y} = 0 \quad \text{at } y = 0, \tag{11}$$

$$u \to 0, \quad T = T_\infty, \quad C = C_\infty \quad \text{as } y \to \infty, \tag{12}$$

where $U = ax$ is the stretching velocity, T_f is the convective fluid temperature below the moving sheet, h_f the convective heat transfer coefficient, $V > 0$ is the velocity of suction and $V < 0$ is the velocity of blowing.

2.2. Method of solution

Introducing the similarity variables as

$$\begin{gathered}\eta = \sqrt{\tfrac{a}{\nu}}y, \quad u = axf'(\eta), \quad v = -\sqrt{a\nu}f(\eta), \\ \theta(\eta) = \tfrac{T-T_\infty}{T_f-T_\infty}, \quad \phi(\eta) = \tfrac{C-C_\infty}{C_\infty},\end{gathered} \tag{13}$$

where η is the similarity variable, $f(\eta)$ is the dimensionless stream function, $\theta(\eta)$ is the dimensionless temperature, $\phi(\eta)$ is the dimensionless concentration and primes denote differentiation with respect to η. The transformed ordinary differential equations are:

$$(1-n)f''' + ff'' - f'^2 + nWef''f''' - Mf' + L_1\left(\theta + N_1\phi\right)\sin\gamma = 0, \tag{14}$$

$$\frac{1}{Pr}\left(1 + \frac{4}{3}R\right)\theta'' + f\theta' + Q_H\theta + Nb\theta'\phi' + Nt\theta'^2 = 0, \tag{15}$$

$$\phi'' + LePrf\phi' + \frac{Nt}{Nb}\theta'' = 0, \tag{16}$$

and the boundary conditions take the following form:

$$f(0) = S, \quad f'(0) = 1, \quad \theta'(0) = Bi\left(\theta(0) - 1\right), \quad Nb\phi'(0) + Nt\theta'(0) = 0, \tag{17}$$

$$f'(\eta) \to 0, \quad \theta(\eta) \to 0, \quad \phi(\eta) \to 0 \quad \text{as } \eta \to \infty, \tag{18}$$

where the prime denotes differentiation with respect to η, $M = \frac{\sigma B^2}{\rho a}$ is the magnetic parameter, $We = \sqrt{\frac{2a}{\nu}}\Gamma U$ is the Weissenberg number, $S = -\frac{V}{\sqrt{a\nu}} > 0$ or (< 0) is the suction (or blowing) parameter, $L_1 = \frac{g\beta_T(T_f - T_\infty)}{a^2 x}$ is the mixed convection parameter, $N_1 = \frac{\beta_C C_\infty}{\beta_T(T_f - T_\infty)}$ is the buoyancy parameter, $R = \frac{4\delta^* T_\infty^3}{kk^*}$ is the radiation parameter, $Pr = \frac{\mu c_p}{k}$ is the Prandtl number, $Le = \frac{\alpha}{D_B}$ is Lewis number, $\alpha = \frac{k}{\rho c_p}$ is the thermal diffusivity, $Bi = \frac{h_f}{k}\sqrt{\frac{\nu}{a}}$ is the Biot number, $Q_H = \frac{Q}{a\rho c_p}$ is the heat source/sink parameter, $Nb = \frac{\tau D_B C_\infty}{\nu}$ is the Brownian motion parameter, $Nt = \frac{\tau D_T(T_f - T_\infty)}{T_\infty \nu}$ is the thermophoresis parameter. The important physical quantities of this problem are the skin friction coefficient C_{f_x} and the local Nusselt number Nu_x, which represent the wall shear stress and the heat transfer rate respectively.

The skin friction coefficient C_{f_x} is given by

$$C_{f_x} {Re_x}^{\frac{1}{2}} = \left((1-n)f''(\eta) + \frac{n}{2} We \left(f''(\eta)\right)^2\right)_{\eta=0}, \tag{19}$$

and the local Nusselt number Nu_x is given by

$$Nu_x {Re_x}^{-\frac{1}{2}} = -\left(1 + \frac{4}{3}R\right)\theta'(0). \tag{20}$$

Here $Re_x = \frac{Ux}{\nu}$ is a local Reynold number.

3. Numerical procedure

The set of coupled nonlinear ordinary differential equations (14) - (16) along with the boundary conditions (17) and (18) are solved numerically by the Runge-Kutta fourth order method with shooting technique. The step size taken as $\Delta\eta = 0.01$ is used to obtain the numerical solution, and the boundary condition $\eta \to \infty$ is approximated by $\eta_{max} = 10$. The solutions are obtained with an absolute error tolerance of 10^{-6} in all cases. In order to get a clear insight of physical problem, numerical results are displayed with the help of graphical illustrations. Also, to calculate the accuracy of the present numerical results, comparison with those obtained by Fathizadeh et al. (2011) are shown in Table 1.

Table 1. Values of skin friction coefficient for several values of magnetic parameter M in the absence of $n = R = Q_H = Bi = S = \gamma = Nb = Nt = Le = 0$.

M	Numerically	HPM [Fathizadeh et al. (2011)]	Present study
0	-1	-1	-1.0000008
1	-1.41421	-1.41421	-1.414214
5	-2.44948	-2.44948	-2.44949
10	-3.31662	-3.31662	-3.316625

4. Results and discussion

This section is focused on the physical insight of different parameters on the velocity $f'(\eta)$, temperature $\theta(\eta)$ and nanoparticle volume fraction profiles $\phi(\eta)$. Figure 1 indicates the effect of the

power law index n on the velocity, temperature and nanoparticle volume fraction profiles. Here, the velocity and the associated boundary layer thickness show reducing but the reverse behavior is obtained for temperature and nanoparticle volume fraction profiles with larger values of the power law index n. The effect of the magnetic parameter M on the velocity, temperature and nanoparticle volume fraction profiles are shown in Figure 2. It is seen that the velocity is a decreasing function of the magnetic field parameter M. It holds because with the increase in M, the Lorentz force increases which produces the retarding effect on the fluid velocity. The effect of magnetic field is to enhance the temperature and nanoparticle volume fraction profiles. Clearly, larger magnetic parameter yields larger Lorentz force which causes strong resistance in the fluid motion. Hence, more heat is produced which enhances the temperature and nanoparticle volume fraction profiles.

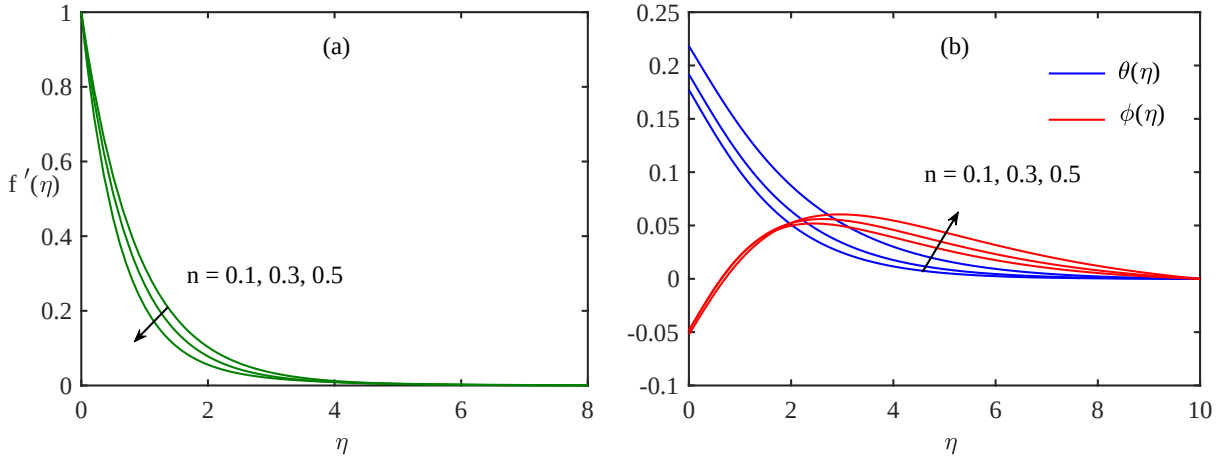

Figure 1. Effect of n on (a) velocity and (b) temperature and nanoparticle volume fraction profiles.

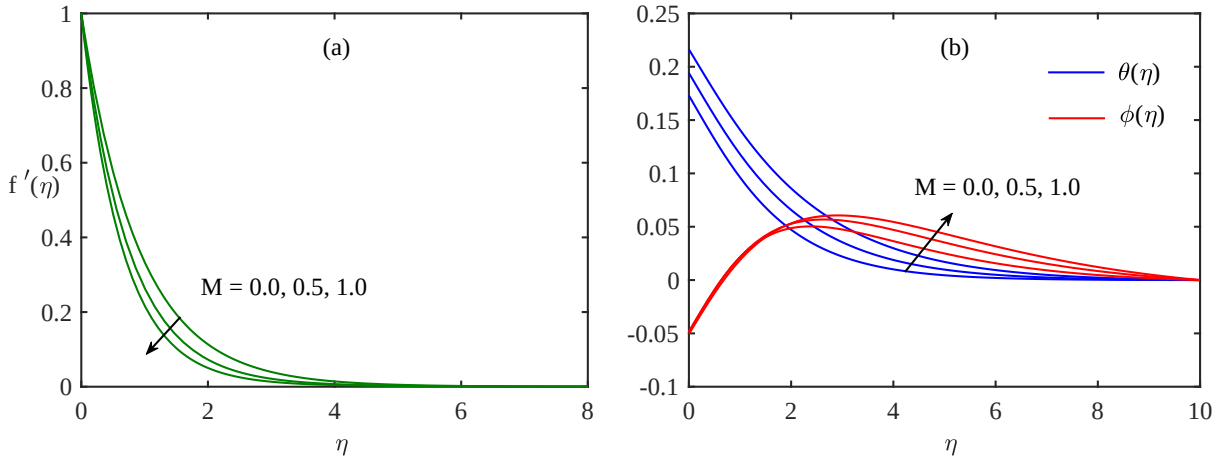

Figure 2. Effect of M on (a) velocity and (b) temperature and nanoparticle volume fraction profiles.

The effects of the suction/blowing parameter S on the velocity, temperature and nanoparticle volume fraction profiles have been analyzed and the results are presented in Figure 3. These figures show that the suction/blowing has a profound effect on the boundary layer thickness in which the suction reduces the thermal boundary layer thickness whereas blowing thickens it. However, the net effect for the suction parameter is to slow down the flow velocity, temperature and nanoparticle

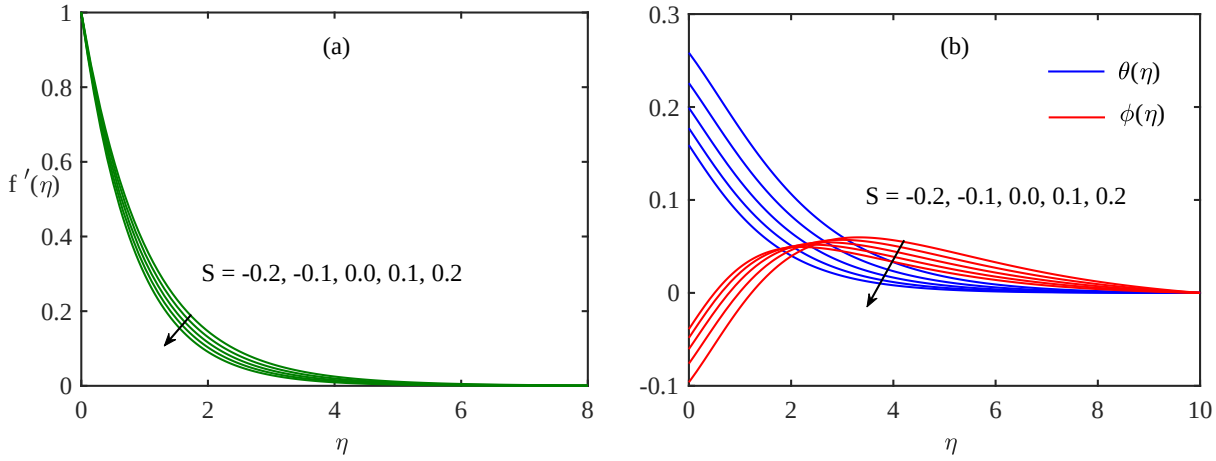

Figure 3. Effect of S on (a) velocity and (b) temperature and nanoparticle volume fraction profiles.

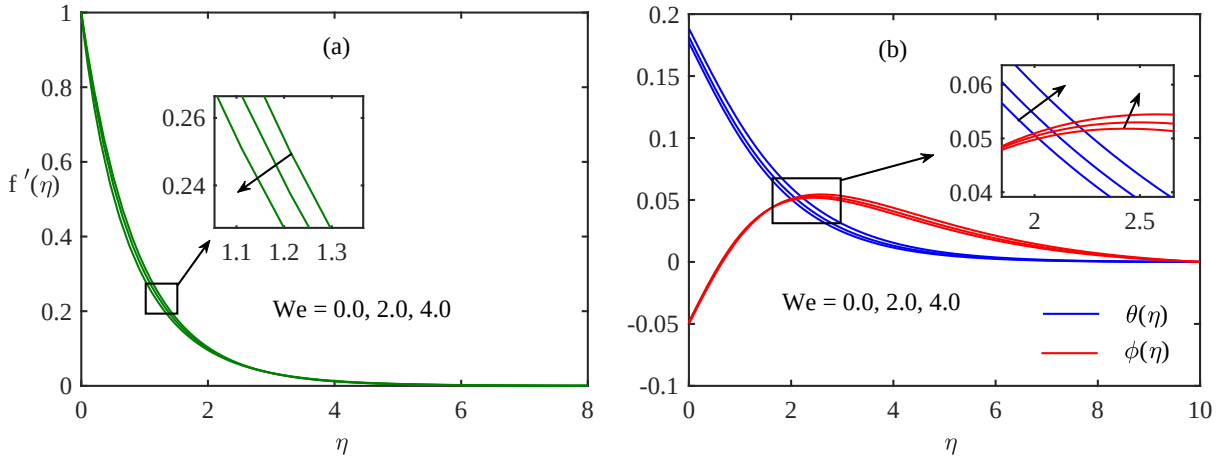

Figure 4. Effect of We on (a) velocity and (b) temperature and nanoparticle volume fraction profiles.

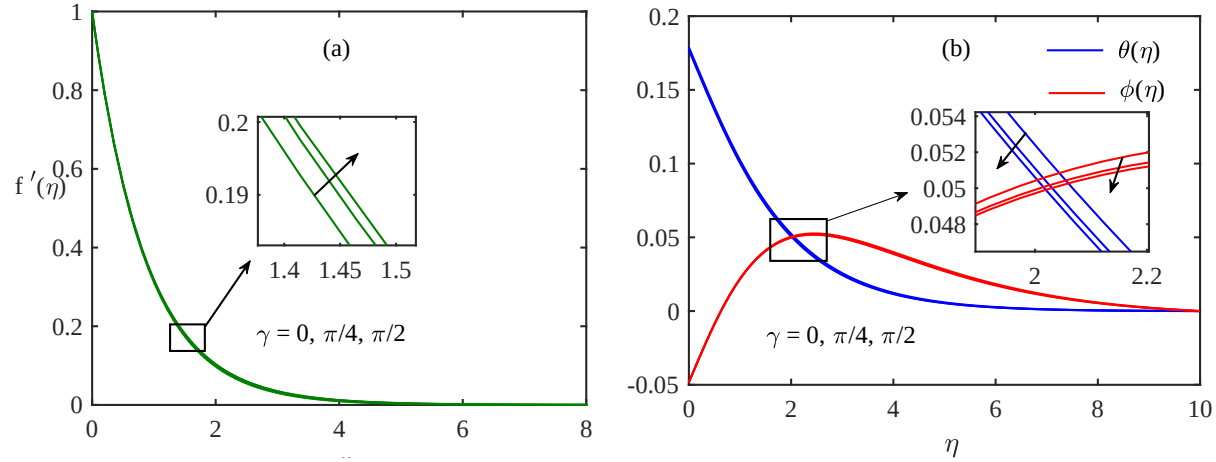

Figure 5. Effect of γ on (a) velocity and (b) temperature and nanoparticle volume fraction profiles.

volume fraction but the reverse is true for the blowing parameter. So, we can conclude that the suction can be effectively used for the fast cooling of the sheet. Figure 4 indicates the effect of the Weissenberg number We on the velocity, temperature and nanoparticle volume fraction profiles. It is observed that the velocity profile decreases by the increasing We. In fact, it is a ratio between the shear rate time and the relaxation time. Hence, for larger Weissenberg numbers We, the fluid becomes thicker, and consequently, the velocity and the boundary layer thickness decrease. Hence velocity profile shows the decreasing behavior while temperature and nanoparticle volume fraction profiles are increasing with increasing values of Weissenberg number We. Figure 5 gives the insight for the influence of the angle of inclination on the velocity, temperature and nanoparticle volume fraction profiles. It is noted that with the increase in γ, the velocity profile increases but the reverse behavior is obtained for temperature and nanoparticle volume fraction profiles.

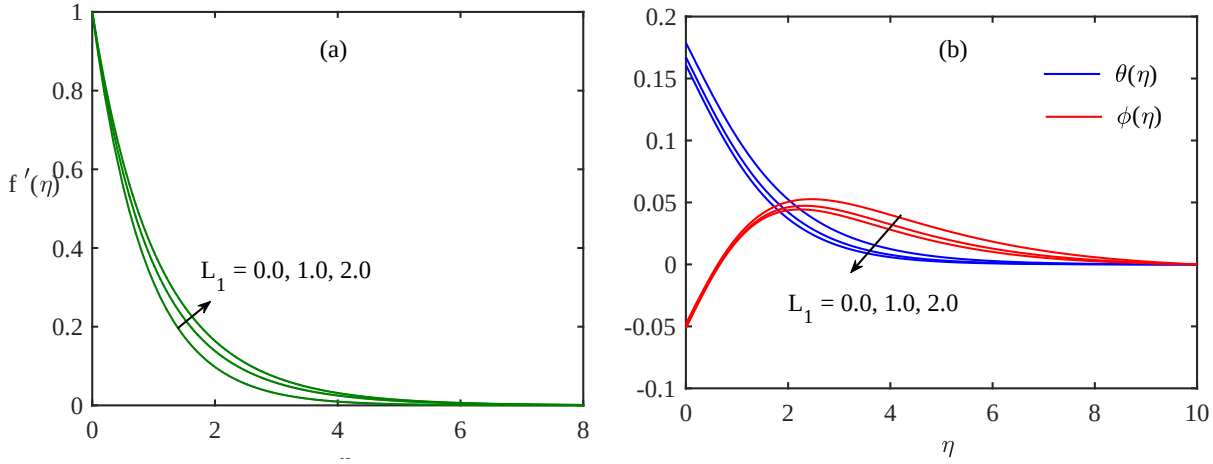

Figure 6. Effect of L_1 on (a) velocity and (b) temperature and nanoparticle volume fraction profiles.

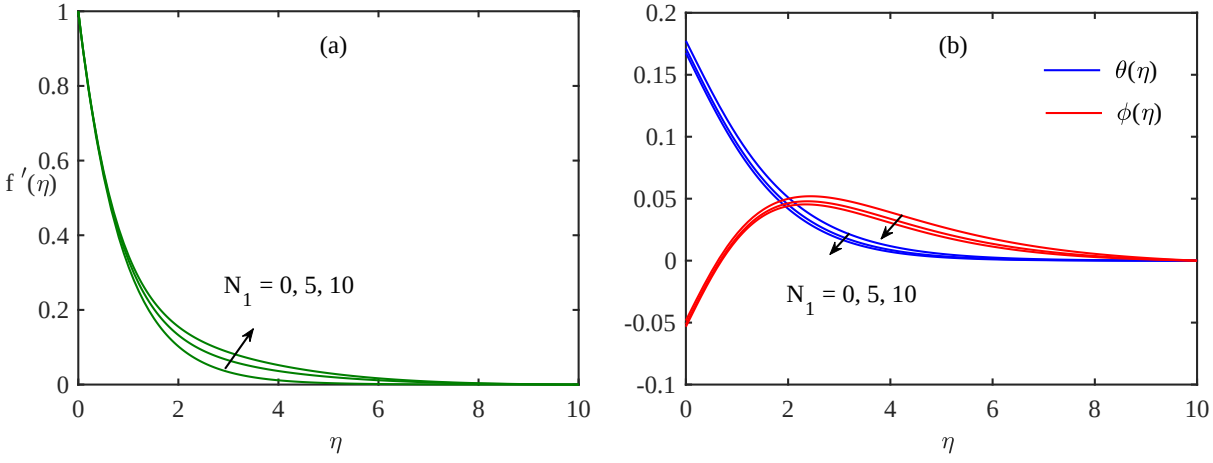

Figure 7. Effect of N_1 on (a) velocity and (b) temperature and nanoparticle volume fraction profiles.

The influence of the mixed convection parameter L_1 on the velocity, temperature and nanoparticle volume fraction profiles are presented in Figure 6. It shows that the velocity profile enhances through the increase in the mixed convection parameter, as the mixed convection parameter is the ratio of the buoyancy to inertial forces. Hence, for larger mixed convection parameters, the

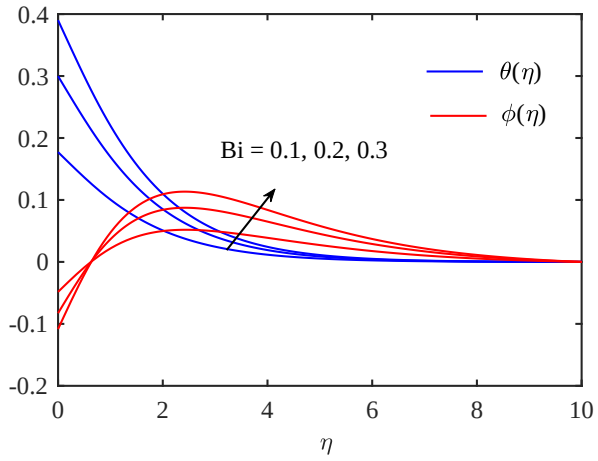

Figure 8. Effect of Bi on temperature and nanoparticle volume fraction profiles.

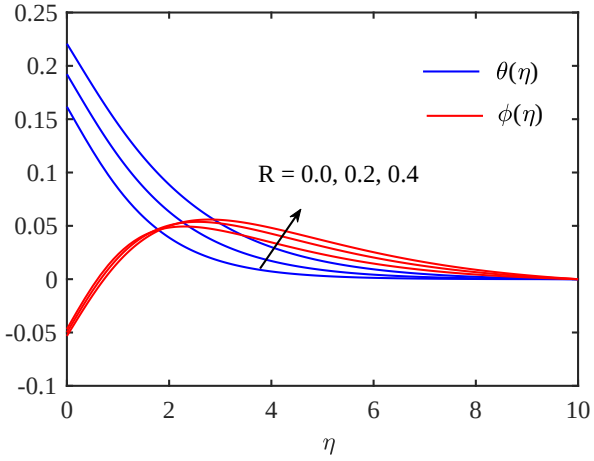

Figure 9. Effect of R on temperature and nanoparticle volume fraction profiles.

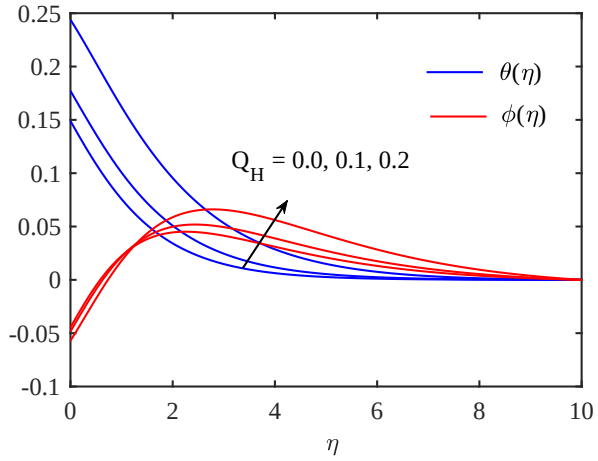

Figure 10. Effect of Q_H on temperature and nanoparticle volume fraction profiles.

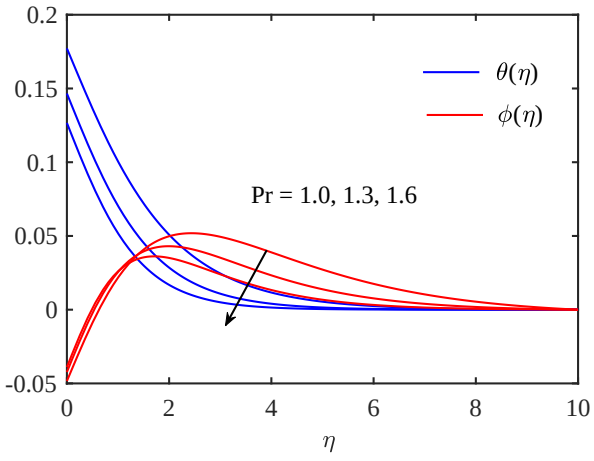

Figure 11. Effect of Pr on temperature and nanoparticle volume fraction profiles.

buoyancy force dominates the inertial force which increases the velocity of the fluid. Moreover, the temperature and nanoparticle volume fraction profiles are decreasing with in increasing values of L_1. Figure 7 displays the effect of the buoyancy parameter N_1 on the velocity, temperature and nanoparticle volume fraction profiles. It is found that the velocity profile and the momentum boundary layer thickness are increasing functions of N_1. The velocity profile shows the emerging behavior near the wall but it increases away from the wall. From this figure the temperature and nanoparticle volume fraction profiles are decreasing for larger values of N_1. Figure 8 shows the impact of convective parameter called Biot number Bi on the temperature and nanoparticle volume fraction profiles. Physically Biot number is the ratio between convection at the surface and conduction within the surface of a body. It holds that both temperature and nanoparticle volume fraction profiles are increasing with an increasing values of biot number. Figure 9 indicates the effect of the thermal radiation parameter R on the temperature and nanoparticle volume fraction profiles. It is seen that the temperature and nanoparticle volume fraction profiles are increasing functions of the radiation parameter R. Figure 10 shows the influence of the heat source/sink parameter on the tem-

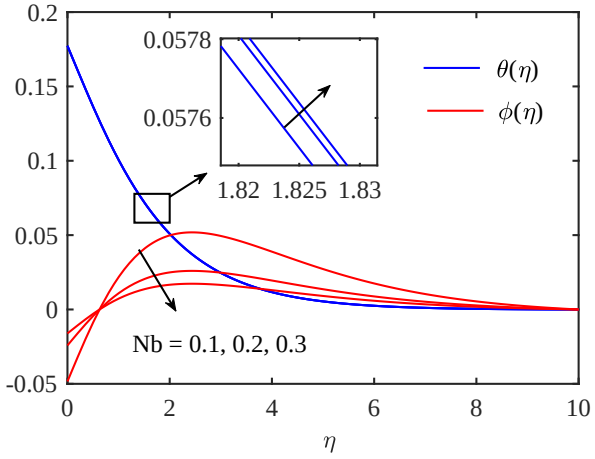

Figure 12. Effect of Nb on temperature and nanoparticle volume fraction profiles.

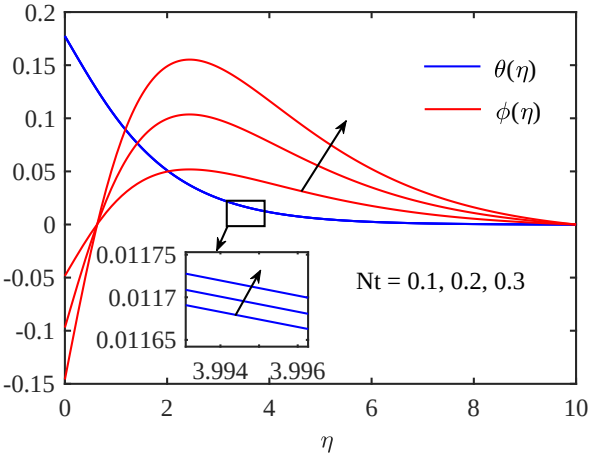

Figure 13. Effect of Nt on temperature and nanoparticle volume fraction profiles.

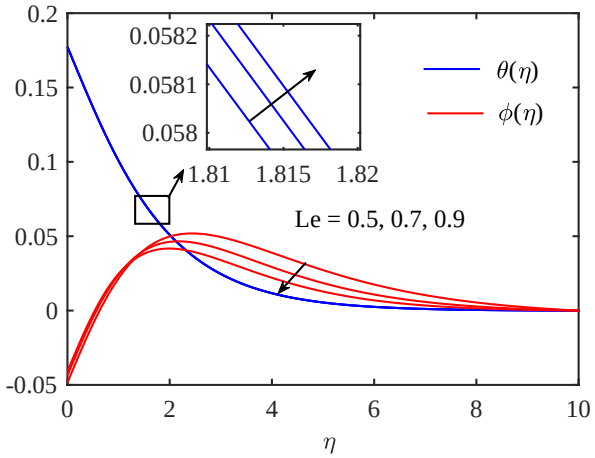

Figure 14. Effect of Le on temperature and nanoparticle volume fraction profiles.

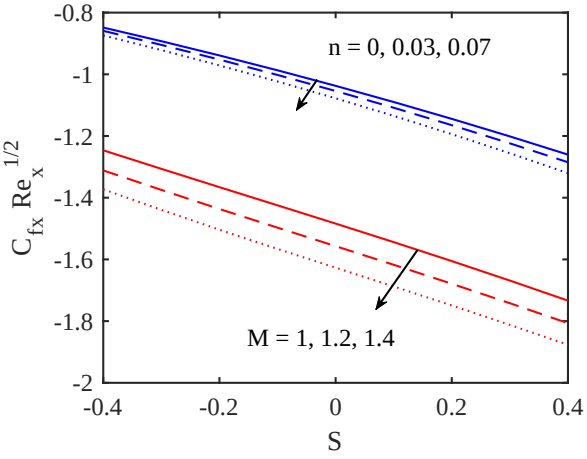

Figure 15. Variation of skin friction with various values of S, n and M.

perature and nanoparticle volume fraction profiles within the boundary layer. From this graph, it is observed that the temperature and nanoparticle volume fraction profiles increase with an increase in the heat source/sink parameter.

Figure 11 demonstrates the behavior of the Prandtl number Pr on the temperature and nanoparticle volume fraction profiles. It is analyzed that the temperature and the thermal boundary layer thickness decrease with an increase in the Prandtl number. In fact, the Prandtl number is the ratio of the momentum diffusivity to the thermal diffusivity. The thermal diffusivity decreases for larger Prandtl numbers. Hence, it causes the reduction in the temperature profile. Moreover from this figure nanoparticle volume fraction profile is also decreasing with larger values of Pr. The behavior of the Brownian motion parameter Nb on the temperature and nanoparticle volume fraction profiles are drawn in Figure 12. It is seen that the temperature profile is increasing but reverse behavior is obtained for nanoparticle volume fraction profiles with increasing values of the Brownian motion parameter Nb. This is because that the random motion of the particles enhances by increasing the Brownian motion parameter Nb and, as a result, the temperature profile increases. Figure

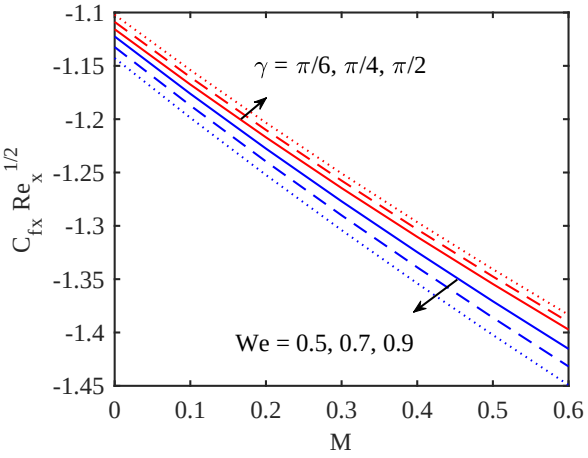

Figure 16. Variation of skin friction with various values of M, We and γ.

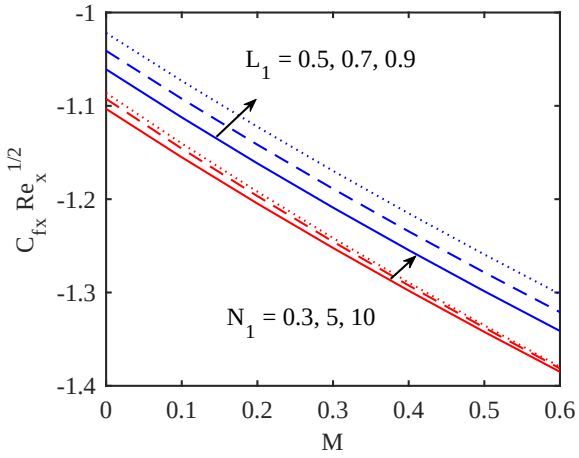

Figure 17. Variation of skin friction with various values of M, L_1 and N_1.

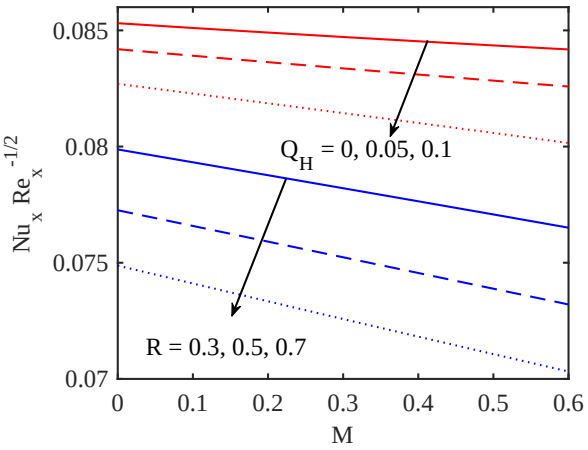

Figure 18. Variation of Nusselt number with various values of M, R and Q_H.

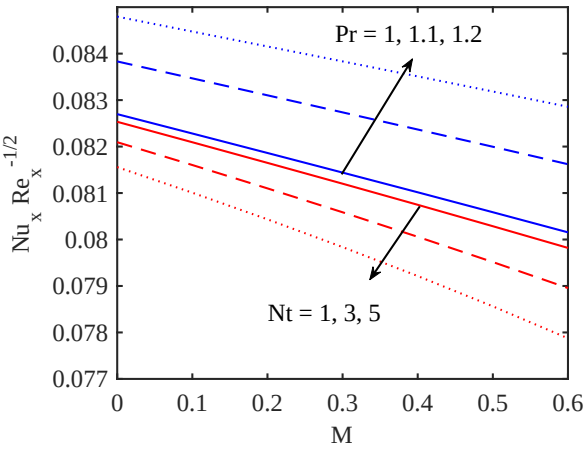

Figure 19. Variation of Nusselt number with various values of M, Pr and Nt.

13 gives the insight for the influence of the thermophoresis parameter Nt on the temperature and nanoparticle volume fraction profiles. The increase in the thermophoresis parameter Nt leads to the enhancement of both the temperature and nanoparticle volume fraction profiles. The difference between the wall and reference temperatures increases for larger Nt, and the nanoparticles move from hot region to cold region. Hence, the temperature profile increases. Figure 14 reveals the variation of temperature and nanoparticle volume fraction profile with coordinate η for various values of Lewis number Le. It is clear from the figure nanoparticle volume fraction profile decreases with an increase in Lewis number, but temperature profile increases. An increase in the values of Lewis number Le corresponds to a weak Brownian diffusion coefficient which results in short penetration depth for nanoparticle volume fraction profile. As a result a rise in Le the nanoparticle volume fraction decreases. It is also noticeable that the nanoparticle volume fraction profile is affected more even for small value of Lewis number Le.

In order to determine the impact of viscous forces at the surface, skin friction is analyzed in Figures 15, 16 and 17 with respect to the variation of suction/blowing parameter S, power law index n,

magnetic parameter M, Weissenberg number We, inclination angle γ, mixed convection parameter L_1 and buoyancy parameter N_1. It is observed that skin friction depicts the decreasing behavior for both blowing and suction region. From these figures local skin friction is decreasing with various values of power law index n, magnetic parameter M and Weissenberg number We but reverse behavior for various values of inclination angle γ, mixed convection parameter L_1 and buoyancy parameter N_1. In Figures 18 and 19, variation is obtained for local Nusselt number with magnetic parameter, radiation parameter, heat source/sink parameter, Prandtl number and thermophoresis parameter. It is seen that the local Nusselt number is decreasing with increasing values of magnetic parameter, radiation parameter, heat source/sink parameter and thermophoresis parameter, but reverse behavior is obtained for Prandtl number.

5. Conclusion

In this paper, we studied the effect of thermal radiation and heat source/sink on MHD boundary layer flow of tangent hyperbolic nanofluid over an inclined stretching sheet with suction/blowing and covective boundary condition. The main findings of this study are as follows:

- The surface temperature of a sheet increases with radiation parameter R. This phenomenon is ascribed to a higher effective thermal diffusivity.
- Inclined angle γ enhances the velocity profile, but it decreases the temperature and nanoparticle volume fraction profiles.
- Velocity profile decreases with increasing magnetic parameter M but temperature and nanoparticle volume fraction profiles are increases in this case.
- The mixed convection parameter L_1 enhances the velocity field, while it reduces the temperature and nanoparticle volume fraction profiles.
- As the thermophoresis parameter Nt enhances, both temperature and nanoparticle volume fraction profiles increases. The effect of Brownian motion Nb is to increase the temperature and decrease the nanoparticle volume fraction profiles.
- The skin friction increases with the increasing values of mixed convection parameter L_1 and buoyancy parameter N_1.
- The local Nusselt number decreases with the increasing values of radiation parameter R and thermophoresis parameter Nt.

REFERENCES

Akbar, N.S., Nadeem, S., Haq, R.U. and Khan Z.H. (2013). Numerical solutions of Magneto-hydrodynamic boundary layer flow of tangent hyperbolic fluid towards a stretching sheet, Indian. J. Phys., Vol. 87, pp. 1121–1124.

Akram, S. and Nadeem, S. (2014). Consequence of nanofluid on peristaltic transport of a hyperbolic tangent fluid model in the occurrence of apt (tending) magnetic field, J. Magnetism. Magnetic. Mater., Vol. 358, pp. 183–191.

Bala Anki Reddy, P. (2016). Magnetohydrodynamic flow of a Casson fluid over an exponentially inclined permeable stretching surface with thermal radiation and chemical reaction, Ain Shams Eng. J., Vol. 7, pp. 593–602.

Bhattacharyya, K., Mukhopadhyay, S. and Layek, G.C. (2013). Similarity solution of mixed convective boundary layer slip flow over a vertical plate, Ain Shams Eng. J., Vol. 4, pp. 299–305.

Buongiorno, J. (2010). Convective Transport in Nanofluids, J. Heat Transfer, Vol. 128, pp. 240–250.

Choi, S.U.S. (1995). Enhancing thermal conductivity of fluids with nanoparticle, Developments and Applications of Non-Newtonian Flows American Society of Mechanical Engineers, Central Michigan University, Vol. 231, pp. 99–105.

Crane, L.J. (1970). Flow past a stretching plate, Z. Angew. Math. Phys., Vol. 21, pp. 645–647.

Elbashbeshy, E.M.A. (2001). Heat Transfer over an Exponentially Stretching Continuous Surface with Suction, Archives of Mechanics, Vol. 53, pp. 643–651.

Fathizadeh, M., Madani, M., Khan, Y., Faraz, N., Ahmet, Y. and Tutkun, S. (2011). An Effective Modification of the Homotopy Perturbation Method for MHD Viscous Flow over a Stretching Sheet, J. King. Saud. University Sci., Vol. 25, pp. 107–113.

Friedman, A.J., Dyke, S.J. and Phillips, B.M. (2013). Over-driven control for large-scale MR dampers, Smart. Mater. Struct., Vol. 22 (045001), No. 15.

Gupta, P.S. and Gupta, A.S. (1977). Heat and Mass Transfer on a Stretching Sheet with Suction or Blowing, Canad. J. Chem. Eng., Vol. 55, pp. 744–746.

Hayat, T., Mumtaz, M., Shafiq, A. and Alsaedi, A. (2017). Stratified magnetohydrodynamic flow of tangent hyperbolic nanofluid induced by inclined sheet, Appl. Math. Mech. -Engl. Ed., Vol. 38, No. 2, pp. 271–288.

Hayat, T., Sajid, Q., Ahmad, B. and Waqas, M. (2016). Radiative flow of a tangent hyperbolic fluid with convective conditions and chemical reaction, Eur. Phys. J. Plus, Vol. 131, pp. 422.

Hayat, T., Shehzad, S.A., Qasim, M. and Alsaedi, A. (2014). Mixed convection flow by a porous sheet with variable thermal conductivity and convective boundary condition, Brazilian J. Chem. Eng., Vol. 31, pp. 109–117.

Khan, W.A. and Pop, I. (2010). Boundary-Layer Flow of a Nanofluid Past a Stretching Sheet, Int. J. Heat Mass Transfer, Vol. 53, pp. 2477–2483.

Kumar, K.G., Gireesha, B.J., Krishanamurthy, M.R. and Rudraswamy, N.G. (2017). An unsteady squeezed flow of a tangent hyperbolic fluid over a sensor surface in the presence of variable thermal conductivity, Results in Physics, Vol. 7, pp. 3031–3036.

Kuznetsov, A.V. and Nield, D.A. (2010). Natural convective boundary layer flow of a nanofluid past a vertical plate, Int. J. Therm. Sci, Vol. 49, pp. 243–247.

Kuznetsov, A.V. and Nield, D.A. (2014). Natural convective boundary layer flow of a nanofluid past a vertical plate: a revised model, Int. J. Therm. Sci, Vol. 77, pp. 126–129.

Magyari, E. and Keller, B. (1999). Heat and Mass Transfer in the Boundary Layers on an Exponentially Stretching Continuous Surface, Journal of Physics D: Applied Physics, Vol. 32, pp. 577–585.

Mair, K., Arif, H., Malik, M.Y., Salahuddin, T. and Farzana, K. (2017). Boundary layer flow of MHD tangent hyperbolic nanofluid over a stretching sheet: A numerical investigation, Results in Physics, Vol. 7, pp. 2837–2844.

Nadeem, S. and Akram, S. (2009). Peristaltic transport of a hyperbolic tangent fluid model in an asymmetric channel, Zeitschrift fur Naturforschung A, Vol. 64a, pp. 559–567.

Nadeem, S. and Maraj, E.N. (2013). The mathematical analysis for peristaltic flow of hyperbolic tangent hyperbolic fluid in a curved channel, Commun. Theor. Phys., Vol. 59, pp. 729–736.

Pak, B.C. and Cho, Y. (1998). Hydrodynamic and Heat Transfer Study of Dispersed Fluids with Submicron Metallic Oxide Particles, Exp. Heat Transfer, Vol. 11, pp. 151–170.

Pop, I. and Ingham, D.B. (2001). *Convective heat transfer: mathematical and computational modelling of viscous fluids and porous media*, Pergamon, Amsterdam.

Prabhakar, B., Shankar, B. and Haq, R.U. (2016). Impact of inclined Lorentz forces on tangent hyperbolic nanofluid flow with zero normal flux of nanoparticles at the stretching sheet, Neural. Comput. Applic. doi: 10.1007/s00521-016-2601-4

Rashidi, M.M., Ashraf, M., Rostami, B., Rastegari, M.T. and Bashir, S. (2013). Mixed convection boundary layer flow of a micro polar fluid towards a heated shrinking sheet by homotopy analysis method, Thermal Science, Vol. 20, pp. 21–34.

Sajjad-ur Rehman, Rizwan-ul Haq, Zafar Hayat Khan and Changhoon Lee, (2016). Entropy generation analysis for non-Newtonian nanofluid with zero normal flux of nanoparticles at the stretching surface, J. Taiwan Inst. Chem. Eng., Vol. 63, pp. 226–235.

Sakiadis, B.C. (1961). Boundary-Layer Behavior on Continuous Solid Surfaces: I. Boundary-Layer Equations for Two-Dimensional and Axisymmetric Flow, A.I.Ch.E. Journal, Vol. 7, No. 1, pp. 26–28.

Salahuddin, T., Imad, K., Malik, M.Y., Mair, K., Arif, H. and Muhammad, A. (2017). Internal friction between fluid particles of MHD tangent hyperbolic fluid with heat generation: Using coefficients improved by Cash and Karp, Eur. Phys. J. Plus, Vol. 132, pp. 205.

Wang, L. and Wei, X. (2009). Heat Conduction in Nanofluids, Chaos Solitons Fract., Vol. 39, pp. 2211–2215.

Waqas, M., Bashir, G., Hayat, T. and Alsaedi, A. (2017). On non-Fourier flux in nonlinear stretching flow of hyperbolic tangent material, Neural. Comput. Applic. doi: 10.1007/s00521-017-3016-6

Wubshet, I. (2017). Magnetohydrodynamics (MHD) flow of a tangent hyperbolic fluid with nanoparticles past a stretching sheet with second order slip and convective boundary condition, Results in Physics, Vol. 7, pp. 3723–3731.

Xuan, Y. and Li, Q. (2003). Investigation on Convective Heat Transfer and Flow Features of Nanofluids, J. Heat Transfer, Vol. 125, pp. 151–1553.